PERGAMON

International Journal of Solids and Structures 37 (2000) 3591–3618

INTERNATIONAL JOURNAL OF SOLIDS and STRUCTURES

www.elsevier.com/locate/ijsolstr

Development and application of a crack tip opening displacement-based mixed mode fracture criterion

Michael A. Sutton[a], Xiaomin Deng[a,*], Fashang Ma[a], James C. Newman Jr.[b], Mark James[c]

[a]*Department of Mechanical Engineering, University of South Carolina, Columbia SC 29208 USA*
[b]*NASA Langley Research Center, Mechanics of Materials Branch, Hampton VA 23681 USA*
[c]*Department of Mechanical Engineering, Kansas State University, Manhattan KS 66506 USA*

Received 28 August 1998; in revised form 27 January 1999

Abstract

Consistent with experimental observations, a crack tip opening displacement (CTOD)-based, mixed mode fracture criterion is developed for predicting the onset and direction of crack growth. The criterion postulates that crack growth occurs in either Mode I or Mode II direction, depending upon whether the maximum in either the opening or the shear component of CTOD, measured at a specified distance behind the crack tip, attains a critical value.

The proposed CTOD-based fracture criterion is implemented in two finite element codes to predict the stable tearing behavior of (a) a modified Arcan test specimen made of AL 2024-T3 and (b) a double cantilever beam (DCB) specimen made of AL 7050. Using the measured load-crack extension data as input, results from simulations of stable crack growth along experimentally measured crack paths for the Arcan specimen demonstrate that the CTOD values obtained in the simulations are in excellent agreement with the proposed criterion. Then, using the CTOD criterion as input, simulations of the Arcan and DCB specimens demonstrate that the CTOD fracture criterion successfully predicts (a) load-crack path data for both specimens, (b) load-crack extension behavior for the Arcan specimen and (c) load-load point displacement data for the DCB specimen.

1. Introduction

Ductile fracture of metallic materials generally involves a stable crack growth process prior to the occurrence of unstable crack propagation. Since stable crack growth requires an increasing applied load for continued crack growth, the maximum load-carrying capacity of ductile materials may be

* Corresponding author. Fax: +001-803-777-0106.
E-mail address: deng@engr.sc.edu (X. Deng).

0020-7683/00/$ - see front matter
PII: S0020-7683(99)00055-4

significantly larger than the loading required to initiate crack growth. Thus, conventional assessment methods using the onset of crack extension for estimating the margin of safety for flawed components manufactured from ductile materials are often overly conservative.

A variety of approaches have been proposed to characterize the stable crack propagation process. For example, the *J*-Integral as a function of crack growth (*J*-*R* curve) has a long history of use as a crack growth resistance curve based on the studies Hutchinson and Paris (1979), Paris et al. (1979), and the others (e.g. Begley and Landes, 1972; Clarke et al., 1976). However, recent analytical and experimental research has shown that: (a) J_c is a strong function of specimen geometry (Yang et al., 1993; Chao and Sutton, 1994) and (b) the *J*-*R* curve is not a material property, varying with specimen geometry (Hancock et al., 1993; Roose et al., 1993). In order to use laboratory experimental data to safely extend the life of cracked structures, a *material fracture parameter* which can be used to characterize the stable crack growth process must be developed.

Among the various fracture parameters that have been proposed over the years, crack tip opening displacement (CTOD) has been shown to have potential in quantifying crack tip deformations during stable crack growth. Early work by Well (1961), Rice and Sorensen (1978), Shih et al. (1979) and Kanninen et al. (1979) for Mode I crack extension gave credence to the use of CTOD, or equivalently for Mode I crack extension, crack tip opening angle (CTOA), as a plausible fracture parameter for ductile materials. Computational studies of stable crack growth under Mode I loading were performed by Newman (1977, 1984), Newman et al. (1992) to assess the viability of a CTOA-based fracture criterion for numerical simulation. In addition, Dawicke and Sutton (1994) conducted a series of tests to obtain the critical CTOA value for an aluminum-alloy (2024-T3). These tests were performed on M(T) (middle crack tension) specimens using both optical microscopy and the two-dimensional digital image correlation method (Han et al., 1994, 1995; Bruck et al., 1989; Sutton et al., 1988) to accurately measure CTOA during stable crack growth. They found that the measured CTOA approached a constant value after an initial amount of crack growth approximately equal to the specimen thickness. Dawicke et al. (1995) then used the CTOA criterion in two-dimensional finite element analyses and successfully predicted the crack-growth behavior of these test specimens.

The studies of CTOD-based fracture criterion mentioned above were confined to Mode I crack extension along a fixed direction which closely approximated the initial crack line. The previous work does not answer the important questions, "In what direction and at what loading will a stationary crack or a stable growing crack propagate under mixed mode loading?" Over the years, a variety of fracture criteria have been proposed to answer these questions, including among others the maximum circumferentical stress criterion (Erdogan and Sih, 1963), referred to as the MCS criterion, the maximum energy release rate criterion (Palaniswamy and Knauss, 1978; Nuismer, 1975), the stationary strain energy density criterion (Sih, 1974), and the $J_{II}=0$ (Pawliska et al., 1993) and $K_{II}=0$ (Cotterell and Rice, 1980; Sumi et al., 1985) criteria. In many cases, the theories proposed have adequately described the direction of crack growth for Mode I-type dominated fracture under mixed mode loading. However, the experimental studies of Maccagno and Knott (1991), Maccagno and Knott (1992) show that ductile fracture mechanism under mixed mode I/II load can be divided into two extremes of behavior, i.e. microvoid coalescence and fast shear, respectively. They found that in fast shear fracture of steel, the initial crack propagation is along the direction with maximum shear stress, and suggested that maximum circumferential stress and shear stress may be the appropriate fracture parameters for void coalescence-type fracture and shear-type fracture, respectively. Hallback and Nilson (1994) used both the maximum circumferential stress and the maximum plastic strain to predict the two separate fracture responses. More recently, Amstutz et al. (1995a), Amstutz et al. (1995b) have shown experimentally that, for Arcan specimens under varying amounts of mixed mode loading, there is a sharp transition of crack growth behavior from predominantly Mode I type to Mode II type. In Mode II, the crack grows under conditions that are locally shear-type in the crack tip region with the crack tip

opening displacement (CTOD) dominated by the shear component parallel to the crack line. Correlating closely with the physical significance of fracture mechanisms of mixed mode I/II, Sutton et al. (1997a) recently proposed a fracture theory. This theory states that a crack loaded in Mode I will grow in the direction of maximum stress triaxiality, and that a shear type fracture takes place in the direction of maximum effective stress. It also states that the transition from Mode I type to Mode I type crack growth occurs when a critical stress triaxiality is reached. However, these criteria do not predict the conditions that are required for continued crack extension.

Some primitive studies have shown that the CTOD-based fracture criterion can predict the load-crack extension response when crack propagation is forced to follow the experimentally observed crack growth paths (Sutton et al., 1997b). In order to develop a CTOD based fracture criterion for general mixed mode loading conditions, the authors have studied (Ma et al., 1998) the fundamental basis for the CTOD fracture criterion under mixed mode loading through analysis of *initial* crack kinking along arbitrary directions. The work has shown that, along the *initial* crack growth direction, in-plane crack tip deformations and stresses are either nearly Mode I or Model II type. Furthermore, either the opening or shear component of crack opening displacement (perpendicular or parallel to the kinked crack direction, respectively), are a maximum during the *initial* increment of crack propagation. Using this data, *initial* crack growth is predicted to occur in either locally Mode I or locally Mode II direction, depending upon whether the opening or the shear component of CTOD measured at a specified distance behind the crack tip attains the critical value. Transition from Mode I-dominated initial crack growth to Mode II-dominated initial crack growth is predicted to occur when the shear component of CTOD reaches the critical CTOD value first.

In this work, a mixed mode, CTOD-based fracture criterion for prediction of *both initial kinking and stable crack propagation* is outlined and verified through successful prediction of the experimentally observed crack growth behavior for two specimens. The plan of the paper is as follows. First, the generalized CTOD criteria is briefly described, along with results from elastic and small scale yielding elastic-plastic analyses of kinked cracks, to demonstrate the underlying basis for the criterion. Secondly, both the Arcan specimen and the DCB specimen are described, appropriate material properties are provided and the availability of experimental observations during crack growth of both load-crack extension and crack path is outlined. Thirdly, finite element analyses of crack propagtion along experimentally observed crack paths for the Arcan specimen are used to provide additional confirmation of the CTOD-based fracture criterion. Fourthly, the CTOD-based criterion is implemented in the finite element code FRANC2DL and the stable crack propagation behavior of both the Arcan and a double cantilever beam (DCB) specimens is described and results are compared to experimental data. Finally, a discussion and conclusions are provided.

2. Rationale for the CTOD-based mixed mode fracture criterion

Fig. 1(a,b) provide a graphical description of the definition of CTOD used in this work. Conceptually, crack propagation is predicted to occur (a) when the magnitude of CTOD, defined as Δ, at a fixed distance behind the current crack tip reaches a critical value and (b) along the direction where CTOD is a maximum. However, because of the relations between Δ and D (the crack tip opening displacement of the original crack) and their components, the actual crack growth direction can be performed using D and its direction only.

In this section, we will provide a rationale for the use of the CTOD criterion in predicting initial crack kinking by (a) utilizing existing asymptotic solutions for a kinked crack and (b) outlining and developing recent results from a modified boundary-layer analysis for initial crack kinking under small scale yield conditions.

2.1. Linear elastic conditions

As shown in Fig. 1, the crack tip opening displacement for a kinked crack, Δ, defined as the relative displacement of two opposite points on the upper and lower crack surfaces at a distance, r_c, behind the crack tip, can be written;

$$\Delta = \sqrt{\delta_I^2 + \delta_{II}^2} = \Delta_0 \sqrt{k_1^2 + k_2^2}, \tag{1}$$

$$\delta_I = \Delta_0 k_1,$$

$$\delta_{II} = \Delta_0 k_2 \tag{2}$$

and

$$\Delta_0 = \sqrt{\frac{r_c}{2\pi}} \frac{1+\kappa}{\mu}, \tag{3}$$

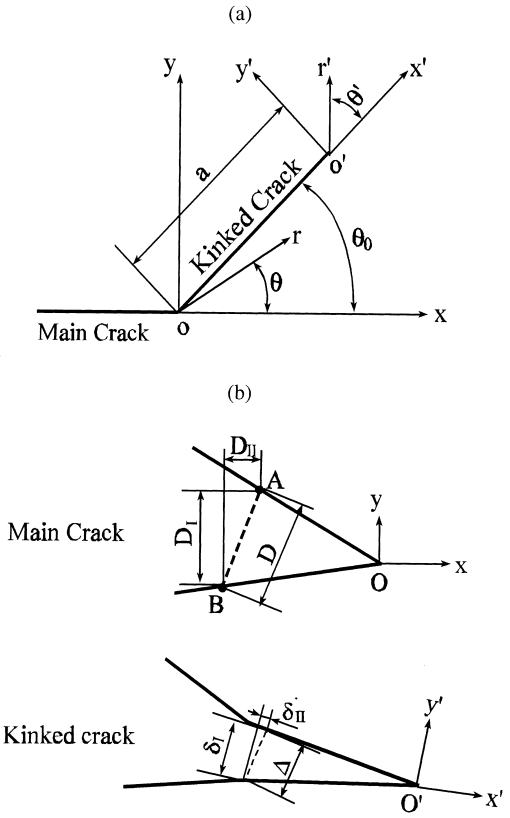

Fig. 1. A geometrical representation of the relation between a main crack and a short kinked crack: (a) coordinate systems for the main and kinked cracks, (b) definitions of crack tip opening displacements for the main and kinked cracks.

where $\mu = E/2(1+\nu)$ is the shear modulus, E the Young's modulus, $\kappa = 3-4\nu$ in plane strain and $\kappa = (3-\nu)/(1+\nu)$ in plane stress, and ν is Poisson's ratio. In the above, k_1 and k_2 are the stress intensity factors of the kinked crack tip, which can be correlated to the stress intensity factors K_I and K_{II} for the main crack in the limit as the length of the kinked crack a shrinks to zero (Nuismer, 1975; Cotterell and Rice, 1980),

$$\left.\begin{aligned} k_1 &= \frac{1}{2}\cos\frac{\theta_0}{2}[K_I(1+\cos\theta_0) - 3K_{II}\sin\theta_0] \\ k_2 &= \frac{1}{2}\cos\frac{\theta_0}{2}[K_I\sin\theta_0 + K_{II}(3\cos\theta_0 - 1)] \end{aligned}\right\}. \tag{4}$$

Thus, k_1 and k_2 depend on the kinking angle for given K_I and K_{II}.

By differentiating Eq. (1) and the expression for δ_I in Eq. (2) with respect to the kinking angle and setting the derivatives equal to zero, it can be shown that the following transcendental equation describes the critical angle for crack kinking under Mode I conditions

$$\frac{\sin\theta_I^c}{3\cos\theta_I^c - 1} = -\frac{K_{II}}{K_I} \tag{5}$$

Defining the energy release rate, G, in terms of Δ and using established expressions for the stress distribution in the vicinity of the main crack for mixed mode I/II conditions (Sih and Liebowitz, 1968), one can perform similar differential operations and show the following. When $\theta_0 = \theta_I^c$, quantities Δ, δ_I, σ_θ, k_1 and G take their respective maximum values, while quantities δ_{II}, $\sigma_{r\theta}$ and k_2 become zero. Thus, under linear elastic and first-order asymptotic conditions (that is, K_I and K_{II} completely describe the crack tip stress and deformation fields), using the maximum in δ_I or Δ as a fracture parameter for the prediction of crack growth is equivalent to using the maxima in commonly accepted fracture criteria (e.g, σ_θ, G, k_I).

By differentiating the expression for δ_{II} in Eq. (2) with respect to the kinking angle and setting the derivatives to zero, one obtains a second transcendental equation for the critical value of $\theta_0 = \theta_{II}^c$:

$$\frac{\cos\frac{\theta_{II}^c}{2}\left(3\cos\theta_{II}^c - 1\right)}{\sin\frac{\theta_I^c}{2}\left(9\cos\theta_I^c + 5\right)} = \frac{K_{II}}{K_I} \tag{6}$$

Following a process that is similar to the one described above for Mode I conditions, one can show that when $\theta_0 = \theta_{II}^c$, the quantities δ_{II}, $\sigma_{r\theta}$ and k_2 are maxima and δ_I, σ_θ and k_1 nearly approach zero. In this case, crack growth would occur in a direction that corresponds to Mode II conditions, where using the maximum in δ_{II} as a fracture parameter for prediction of the direction of crack growth is equivalent to using the maxima in commonly accepted fracture criteria (e.g, $\sigma_{r\theta}$, K_{II}).

Provided that crack growth occurs along directions corresponding to the maxima in key crack tip variables, these results show that the crack tip opening displacement components, δ_I and δ_{II}, are viable fracture parameters for predicting the onset of crack growth under mixed mode loading conditions. Conceptually, the onset of crack growth can be assumed to occur in either the direction θ_I^c or θ_{II}^c, depending on whether $\delta_I = \delta_I^c$ or $\delta_{II} = \delta_{II}^c$ is satisfied first. Here, δ_I^c and δ_{II}^c would be material parameters determined from Mode I and Mode II fracture experiments, respectively.

The conclusions described above used features of the kinked crack tip fields. Referring to Fig. 1(a,b), the following shows how the crack growth direction can be correlated with a local mode mixity parameter defined in terms of the crack tip opening displacement D and its components for the main

crack. Under linearly elastic conditions, the local and remote mode mixities, α and β, respectively, for the main crack tip, can be defined as

$$\alpha = \arctan\left(\frac{D_{II}}{D_I}\right)$$

and

$$\beta = \arctan\left(\frac{K_{II}}{K_I}\right). \tag{7}$$

Under first-order asymptotic conditions, it can be shown that $\alpha = \beta$, since $D_I = D\cos\alpha = \Delta_0 K_I$, and $D_{II} = D\sin\alpha = \Delta_0 K_{II}$. Thus the direction of crack growth, given in Eqs. (5) and (6), under mode-I and mode-II crack growth conditions, respectively, can be expressed in term of the local mode mixity α as;

(Mode I)

$$\frac{\sin\theta_I^c}{3\cos\theta_I^c - 1} = -\tan\alpha$$

and

(Mode II)

$$\frac{\cos\frac{\theta_{II}^c}{2}\left(3\cos\theta_{II}^c - 1\right)}{\sin\frac{\theta_{II}^c}{2}\left(9\cos\theta_{II}^c + 5\right)} = \tan\alpha. \tag{8}$$

Furthermore, the maximum CTOD components (with respect to their dependence on the kinking angle) for a kinked crack can be correlated to the crack tip opening displacement D for the main crack using Eqs. (1)–(4):

$$\left.\begin{aligned}\delta_I &= \frac{D}{2}\cos\frac{\theta_I^c}{2}\left[\cos\alpha\left(1+\cos\theta_I^c\right) - 3\sin\alpha\sin\theta_I^c\right]\\ \delta_{II} &= \frac{D}{2}\cos\frac{\theta_{II}^c}{2}\left[\cos\alpha\sin\theta_{II}^c + \sin\alpha\left(3\cos\theta_{II}^c - 1\right)\right]\end{aligned}\right\}, \tag{9}$$

where the dependence of θ_I^c and θ_{II}^c on α is given in Eq. (8). Fig. 2 presents a graphical description of the relations between $(\delta_I)_{max}$, $(\delta_{II})_{max}$ and α for a range of values for α. Fig. 2 demonstrates that, for all mode mixity values, the maximum value for δ_{II} is always smaller that the maximum value for δ_I. Thus, crack propagation under linear elastic conditions is predicted to occur under only Mode I condition if $\delta_I^c = \delta_{II}^c$.

As a final note, Eqs. (8) and (9) indicate that $(\delta_I)_{max}$ (if $\theta_0 = \theta_I^c$) and $(\delta_{II})_{max}$ (if $\theta_0 = \theta_{II}^c$) are explicit functions of the crack tip opening displacement for the main crack, D, under linearly elastic and first-order asymptotic conditions. Thus, the attainment of a critical value for $(\delta_I)_{max}$, $(\delta_{II})_{max}$ corresponds to a critical value for D. Hence, in this case, it is possible to use CTOD quantities at the main crack tip to assess the direction and onset of crack propagation.

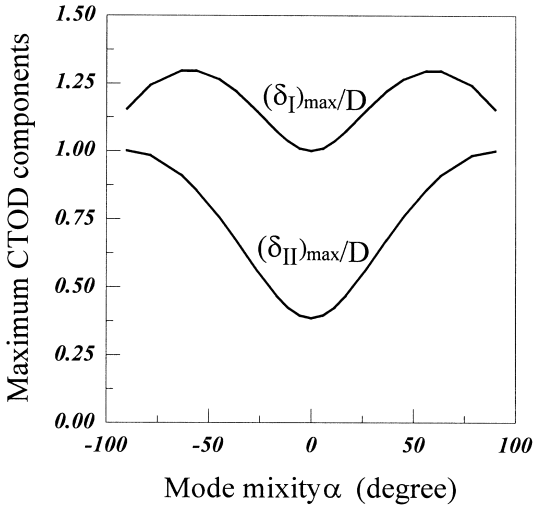

Fig. 2. Maximum values of the CTOD components, δ_I and δ_{II}, of the kinked crack, as functions of the local mode mixity α, under linearly elastic conditions.

2.2. Small scale yielding, elastic-plastic conditions

The small-scale yielding (SSY) model used in this work is shown in Fig. 3, where the focused crack-tip mesh was used to predict the initial crack kinking direction. The finite element analyses in this section were performed using the finite element code ZIP2DL (Deng and Newman, 1997a, 1997b). The remote boundaries are subjected to imposed displacements corresponding to a plane stress modified boundary layer (MBL) formulation (Rice, 1974; Larsson and Carlsson, 1973)

$$u_x = \sqrt{\frac{r_a}{2\pi}}\left[\frac{K_I}{\mu}\cos\frac{\theta}{2}\left(\frac{\kappa-1}{2}+\sin^2\frac{\theta}{2}\right)+\frac{K_{II}}{\mu}\sin\frac{\theta}{2}\left(\frac{\kappa+1}{2}+\cos^2\frac{\theta}{2}\right)\right]+\frac{(1+K)K_{eff}r_a}{8\mu\sqrt{\pi r_a}}B\cos\theta, \quad (10a)$$

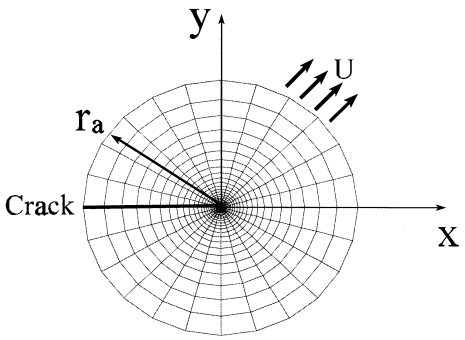

Fig. 3. A small-scale yielding crack-growth model and a typical finite element mesh for the model, where r_a is the radius of the remote boundary with a specified displacement **u**.

$$u_y = \sqrt{\frac{r_a}{2\pi}}\left[\frac{K_I}{\mu}\sin\frac{\theta}{2}\left(\frac{\kappa+1}{2}-\cos^2\frac{\theta}{2}\right)-\frac{K_{II}}{\mu}\cos\frac{\theta}{2}\left(\frac{\kappa-1}{2}-\sin^2\frac{\theta}{2}\right)\right]-\frac{(3-K)K_{eff}r_a}{8\mu\sqrt{\pi r_a}}B\sin\theta. \quad (10b)$$

where

$$B=\frac{T\sqrt{\pi r_a}}{K_{eff}}$$

and

$$K_{eff}=\sqrt{K_I^2+K_{II}^2}. \quad (11)$$

Since the objective of this analysis is to compare the magnitude and component values for CTOD for all kinking angles at a given load, the ability to allow incremental crack growth along various directions was required. For this reason, the focused mesh shown in Fig. 3 includes twelve elements from $-90 < \theta_0 < 90^\circ$. To allow crack growth along each of the thirteen radial lines ahead of the main crack tip, each angle θ_0 in the focused mesh includes a set of node pairs. The applied load is increased gradually until the CTOD criterion is satisfied and the computed CTOD value at a specified distance behind the initial crack tip attains a critical value of $D=D_c$. The crack is then extended along the direction $\theta=\theta_0$ by one element length by allowing the appropriate node pair to separate. This provides the mechanism for determining the critical kinking direction $\theta_0=\theta_c$ with the maximum magnitude of CTOD, the maximum opening component of CTOD, or the maximum shearing component of CTOD.

The SSY numerical analyses were performed for $B=-1$, 0, 1 and $\beta=0^\circ$, -5.7°, -11.3°, -45°, -63°, -84° and -90°. For consistency with forthcoming analyses on the Arcan test specimen, (a) all components of CTOD were calculated at 0.962 mm behind the crack tip, (b) material properties in the SSY model are those of 2024-T3 aluminum, (c) the critical CTOD values are $D_c=0.089$ mm (which corresponds to $D_c=0.0962$ mm at 1 mm behind crack tip) based on the extensive experimental data of Amstutz *et al.*, and (d) each incremental crack growth step was 0.192 mm.

Fig. 4(a) presents the predicted initial crack kinking direction (assuming $\delta_I^c=\delta_{II}^c$) as a function of mode mixity, α, using both linear elastic and SSY analyses. Note that symmetry about the origin can be used to generate the θ_c–α relation for $0 < \alpha < 90^\circ$. The experimental data are for the Arcan specimens, and the conversion between the Arcan test loading angle Φ (see Fig. 6) and the crack tip local mixity α is shown in Fig. 4(b). It can be seen from Fig. 4(a) that the effects of T-stress on the predicted initial crack direction are quite small, suggesting that the CTOD criterion is not sensitive to specimen size and geometry based on the SSY and modified boundary layer (MBL) formulation analyses. Also, the CTOD criterion predicts a transition of initial crack kinking mode from Mode I to Mode II as mode mixity varies from Mode I values to Mode II values. As shown in Fig. 4, this prediction is consistent with recent experimental evidence of Amstutz *et al.* for a 2024-T3 aluminum specimen, where a transition in fracture mode was observed during initial crack kinking for $|\alpha| \cong 70^\circ$. Finally, it is noted that the linear elastic prediction has the correct trends for predicting the initial kinking direction during Mode I crack growth, but it is not capable of predicting the transition to Mode II type crack growth.

To obtain the data shown in Fig. 4, several crack kinking analyses were required to determine the direction and onset of initial crack growth. This process is computationally intensive and would be virtually unusable in solving more complex problems. However, as shown in Eq. (9), it is possible to develop a direct relationship between CTOD at the kinked crack tip and the main crack tip, similar to what was analytically demonstrated for the elastic case.

To obtain the relationship, the dependence (shown in Fig. 4) of the crack growth direction, θ_c (in degrees), on the mode mixity, α (in radians), can be expressed in the following empirical expressions,

$$\left.\begin{aligned}\theta_c = \theta_I^c = a_1 \arctan(b_1\alpha) \text{ for } |\alpha| < \alpha_c \\ \theta_c = \theta_{II}^c = a_2 \cos(b_2\alpha)\frac{\alpha}{|\alpha|} \text{ for } |\alpha| \geq \alpha_c\end{aligned}\right\}, \tag{12}$$

where α_c is regarded as the critical local mixity for the transition of Mode I type fracture to Mode II type fracture and a_1, b_1, a_2 and b_2 are the fitting parameters. For 2024-T3 aluminum, the parameters

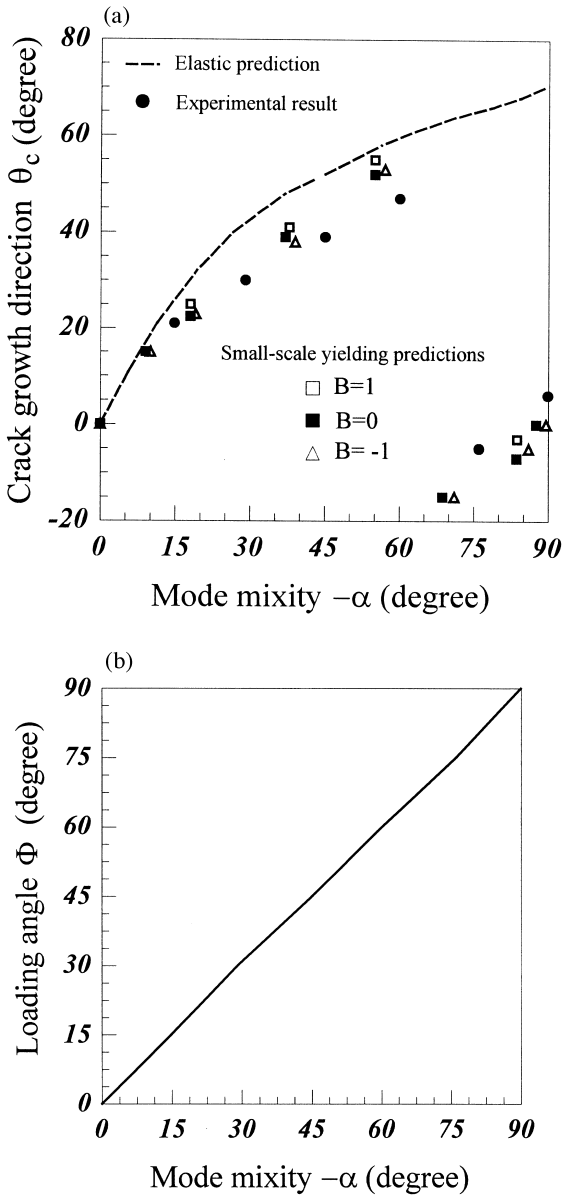

Fig. 4. The crack growth direction θ_c as a function of the local mode mixity α, predicted under both linearly elastic and modified small-scale yielding conditions, and compared with the Arcan test results.

involved in Eq. (12) between the crack growth direction, θ_c, and local mixity, α, are

$$\left.\begin{array}{l}\alpha_c = 70^\circ = 1.222 \text{ rad},\\ a_1 = -36.5, b_1 = 2.2,\\ a_2 = 57.3, b_2 = 1.0.\end{array}\right\}. \tag{13}$$

Next, detailed finite element analyses of crack kinking from a main crack conclusively demonstrate that (a) when the local mode mixity for the main crack $|\alpha| \leq 70^\circ$, the maximum opening component $(\delta_I)_{max}$ is larger than the maximum shearing component $(\delta_{II})_{max}$, and (b) for $|\alpha| > 70^\circ$, the maximum shearing component is $(\delta_{II})_{max}$ larger than the maximum opening component, $(\delta_I)_{max}$. Fig. 5 presents the ratio of $(\delta_I)_{max}$ and/or $(\delta_{II})_{max}$ to the CTOD value, D, for the main crack as a function of mode mixity for the main crack, α. Since Fig. 5 clearly shows that, from $(\delta_I)_{max}/D = (\delta_{II})_{max}/D = \delta_c/D$, the attainment of a critical value δ_c for the kinked crack is equivalent to the total CTOD for the main crack attaining a critical value, i.e. $D = D_c$. Thus, the main crack provides sufficient information for predicting crack growth under mixed mode loading, with the local mode mixity at the main crack tip, α, determining crack growth direction by Eq. (12) and the magnitude of the CTOD value, D, determining the onset of continued crack growth.

In summary, the CTOD criterion has a solid foundation, being directly related to key fracture mechanics parameters. Furthermore, the CTOD criterion has been shown to predict the *initial crack kinking behavior* under both elastic and small scale yielding conditions. However, as with any concept, the assessment of its applicability in predicting *both initiation and stable crack growth* for a wide range of materials and specimen geometry requires direct comparison between experimental observations and theoretical predictions. Due to the expense of large test programs, it has oftentimes been true that the database required for meaningful comparisons is quite limited. Fortunately, recent programs directed towards improving the safety of aerospace travel have included extensive experimental testing for assessing the accuracy of advanced structural models. In particular, a sizable experimental database now exists from testing of Arcan and DCB specimens.

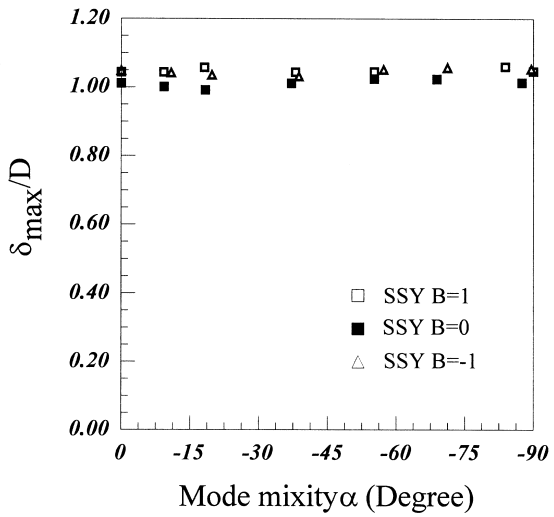

Fig. 5. The maximum crack tip opening displacement component δ_{max} of the kinked crack relative to the crack tip opening displacement D of the main crack, as a function of the local mode mixity α.

3. Experimental background

The Arcan specimen and test fixture are shown in Fig. 6. Originally used for testing of composite specimens by Arcan et al. (1978), the fixture was modified by Amstutz et al. (1995a, 1995b) for stable tearing tests. In particular, increasing the number of bolts and adding hardened drill rod inserts stiffened the specimen-fixture connection. The 15-5PH stainless-steel test fixture is nominally 19 mm thick and was machined to test 2.3 mm thick specimens. The locations of pinholes on the outer edge of the fixture provide a range of loading angles, Φ, which results in a full spectrum of mode mixities. The test specimens were machined from 2024-T3 aluminum plates, with a fixed crack length, a, to width, w, ratio of $a/w = 0.167$.

The material properties for 15-5PH stainless steel are Young's modulus, $E = 207$ GPa, Poisson's ratio, $\nu = 0.3$ and $\sigma_y = 1.72$ GPa. For 2024-T3 aluminum, $E = 71.2$ GPa, $\nu = 0.3$ and $\sigma_y = 344.5$ MPa. The strain hardening curves for 15-5PH and 2024-T3 aluminum are shown in Fig. 7 in terms of the effective plastic flow stress and the effective plastic strain.

The stable tearing tests for the Arcan test specimen resulted in a wide range of crack growth data for all loading angles, Φ. Specifically, the database includes measurements of (a) D, D_{I} and D_{II}, (b) load-

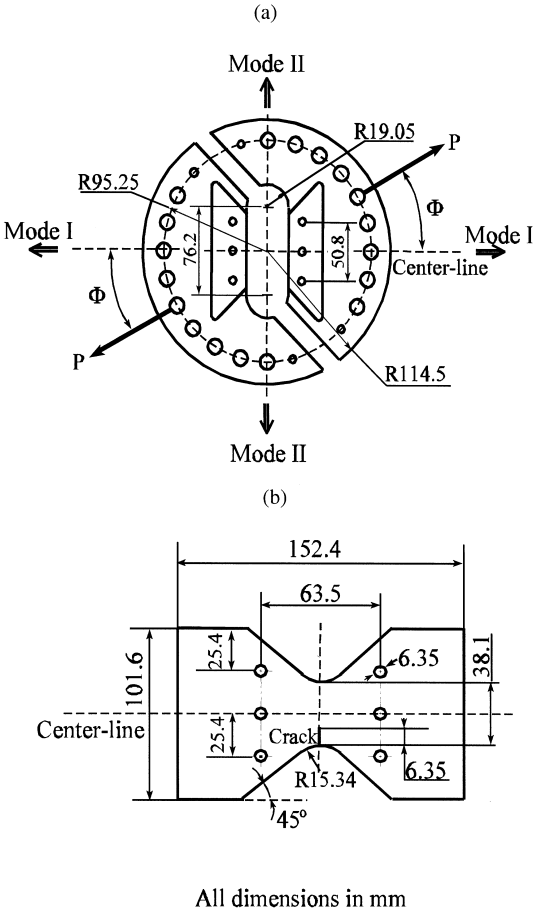

Fig. 6. A schematic of (a) the modified Arcan fixture and (b) the Arcan specimen.

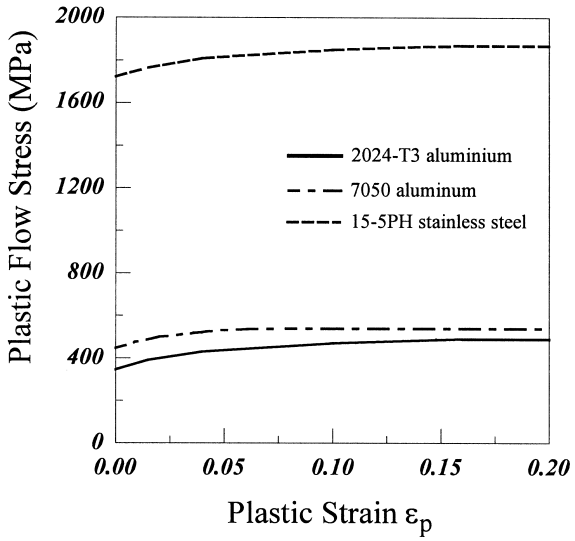

Fig. 7. Strain hardening curves for 15-5PH stainless steel, 2024-T3 aluminum, and 7050 aluminum.

crack extension and (c) load-crack path. The range of data available provides the opportunity to perform additional simulations for assessing the robustness of the CTOD criterion.

Recently, Pettit (1998) performed a series of crack tearing experiments on DCB specimen made from 7050 aluminum. The DCB specimen is shown in Fig. 8. The test specimens are 2.34 mm thick and are machined from 7050 aluminum plate, with in-plane dimensions a/w varying from 0.171 to 0.545. The material properties for 7050 aluminum are $E = 73.7$ GPa, $\nu = 0.3$ and $\sigma_y = 448$ MPa. The strain-hardening curve is shown in Fig. 7 in terms of the effective plastic flow stress and the effective plastic strain. The database generated by the DCB stable tearing tests includes measurements of (a) load-load point displacement and (b) load-crack path throughout the crack growth process for all a/w values.

4. Numerical simulation of crack growth using the CTOD criterion

A series of simulations will be performed in this paper. First, crack growth along measured crack

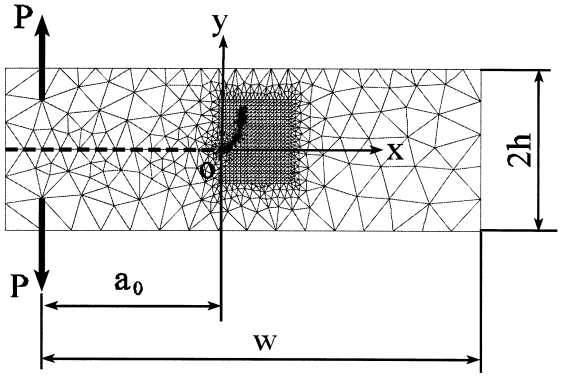

Fig. 8. The geometry, size, and finite element mesh of a DCB specimen.

paths in the Arcan specimen will be performed to confirm that crack growth throughout the total crack propagation process is always under either Mode I or Mode II conditions. Secondly, both the direction and onset of crack growth will be predicted for both the Arcan and the DCB specimens using only the CTOD-based fracture criterion. Direct comparisons of the measured and predicted load-crack extension data, load-crack path data and load-load point displacement will be presented.

4.1. Crack growth simulations for Arcan specimen with specified crack path

The primary objective of these analyses is *to generalize the elastic and SSY elastic-plastic results*. In particular, the finite element simulations of crack growth along the experimentally observed crack growth paths demonstrates that crack propagation occurs under either Mode I or Mode II conditions throughout the entire crack growth history, with the satisfaction of $D = D_c$ accurately predicting the onset and direction of crack growth under mixed mode conditions.

Using the experimentally measured crack propagation paths of Amstutz et al. (1995a, 1995b), as shown in Fig. 9 for different loading angles, Φ, a series of finite element models similar to the one shown in Fig. 10 were generated for input to ZIP2DL. The test specimen and fixture are modeled as a single, continuous component in both simulations. For crack propagation along experimentally observed crack paths, a typical mesh used in ZIP2DL for $\Phi = 45^\circ$ is composed of 2,700 four-node quadrilateral, plane stress elements; 2,000 elements are used in the specimen region and 700 elements in the fixture region. Smaller elements, on the order of 0.192 mm, are distributed along the measured crack-growth path. Load is applied at the appropriate angle by locating a nodal point at the correct angle and position in the mesh.

Crack growth was controlled using the measured load-crack extension data of Amstutz *et al*, with crack growth increments of 0.192 mm throughout the crack growth process. The applied load is incrementally increased until the CTOD at a distance $r_c = 0.96$ mm behind the crack tip attains the experimentally observed averaged value, 0.089 mm. The crack tip node pair is released and equilibrium with a new crack length is iteratively computed. The details of the numerics used in the crack growth process for ZIP2DL are outlined by Deng and Newman (1997b). This process continues until the desired crack extension is obtained. During the crack growth process, δ_I and δ_{II} are calculated at each step of crack growth at 0.96 mm behind the current crack tip.

Fig. 11 shows δ_I and δ_{II} as a function of crack growth for $\Phi = 0^\circ$, 15°, 45°, 75° and 90°. Throughout the crack growth process, it is observed that (a) δ_I is dominant for $\Phi < 75^\circ$ ($\delta_I \cong 0.085$ mm and $\delta_{II} = 0$ except during the initial stages of crack propagation), indicating a mode I type of crack growth, and (b) δ_{II} is dominant for $\Phi \geq 75^\circ$ ($\delta_{II} \cong 0.080$ mm $\Phi = 75^\circ$ and $\delta_{II} \cong 0.090$ mm for $\Phi = 90^\circ$), indicating a mode II type of crack growth. The results are in excellent agreement with experimental observations of Amstutz et al. (1995a), Amstutz et al. (1995b), where the average measured CTOD value was 0.089 mm and the measured local CTOD values were either Mode I or Mode II during crack growth. These results demonstrate that crack growth occurs under either local Mode I or local Mode II conditions, implying that δ_I and δ_{II} are appropriate crack growth parameters. Since δ_I and δ_{II} can be related to D_I and D_{II} for the main crack, efficient implementation of the CTOD fracture criterion will employ main crack values to eliminate the requirement for multiple crack kinking analyses for prediction of the crack growth direction.

4.2. Crack growth simulations without specified paths

4.2.1. Finite element models and fracture criterion

Using the observation that D_I, D_{II} and D values obtained from the main crack at any load can be used to predict both the direction and onset of crack growth, the CTOD based mixed mode fracture

criterion is relatively easy to implement in conventional finite element algorithms. Thus, CTOD and its components at a distance r_c behind the current crack tip can be obtained from the difference in the displacement vectors for corresponding points on the upper and lower surfaces of the crack at each step of increasing loading. (In this work, r_c is an integral multiple of the near-crack-tip uniform element size.) At the Nth nodal pair behind crack tip node, one has:

$$D_{\mathrm{I}} = u_y(N\text{th nodal pair}^+) - u_y(N\text{th nodal pair}^-), \tag{14a}$$

$$D_{\mathrm{II}} = u_x(N\text{th nodal pair}^+) - u_x(N\text{th nodal pair}^-), \tag{14b}$$

$$D = \sqrt{D_{\mathrm{I}}^2 + D_{\mathrm{II}}^2}$$

and

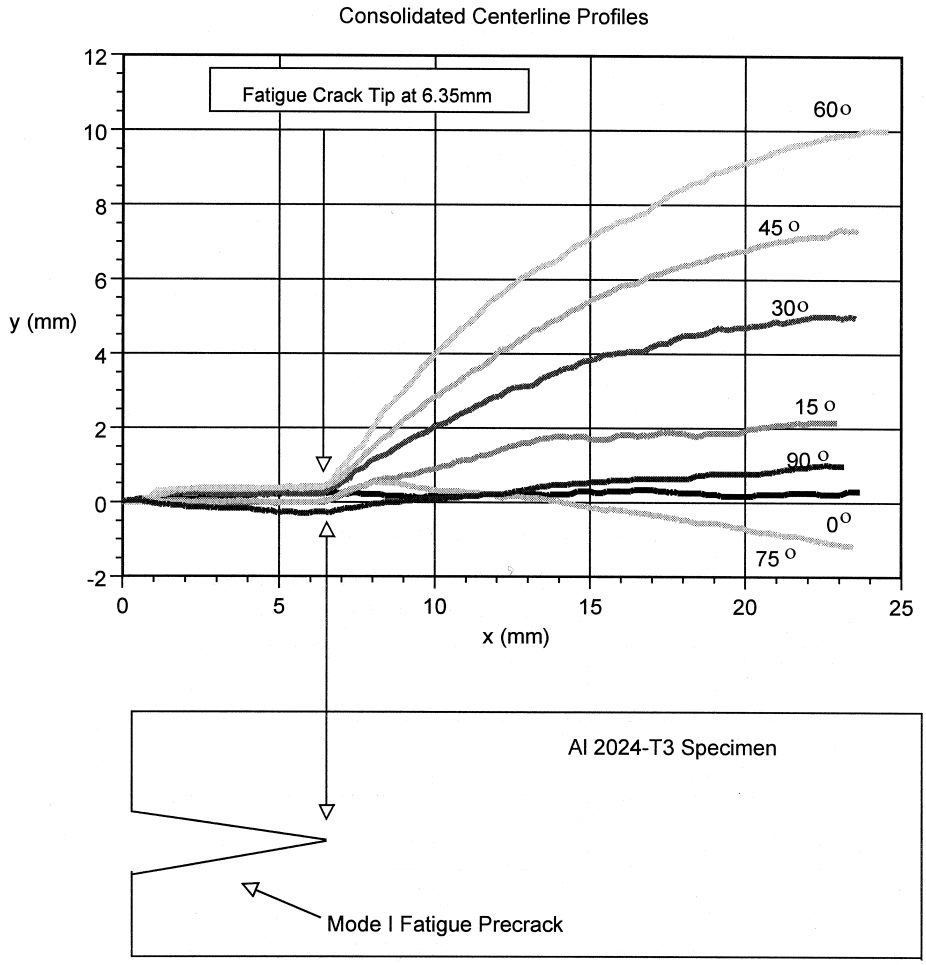

Fig. 9. Experimentally observed crack growth paths in Arcan specimens for a spectrum of mixed mode loading angles.

$$\alpha = \arctan \frac{D_{II}}{D_I}. \tag{14c}$$

where subscript '+' and '−' means the nodal pair point is located on the upper and lower surfaces of the crack, respectively. Using Eqs. (12), (13) and (14), the onset and direction of crack growth can be determined under general, mixed-mode loading conditions.

To predict the crack growth behavior, including crack path and loading response, the CTOD mixed mode fracture criterion described above is implemented in the finite element code, FRANC2DL (Swenson and James, 1997; James and Swenson, 1998). In FRANC2DL, when the fracture criterion is satisfied, automatic re-meshing algorithms extend the crack in the predicted direction, and automatic mapping algorithms transfer state variables from the old mesh to the new one. In this manner, crack propagation can be simulated in arbitrary directions, as specified by the CTOD fracture criterion. Details of the numerical analysis procedure used in the crack growth process for FRANC2DL are outlined in references cited above.

In the crack growth simulations, six-node triangular elements are used for both the Arcan and DCB specimens. Fig. 12 presents the local meshes in the crack tip region for the Arcan specimens, with the smallest element size of 0.5 mm along the crack front. Extensive numerical simulations using the CTOD criterion for crack growth in aluminum material has shown that the near-tip mesh size is appropriate (see Newman et al., 1992). These meshes are used to predict crack propagation for a variety of loading angles. When the CTOD value at the second node behind crack tip (which is at a distance of 1 mm) attains a critical value, the fracture criterion predicts the crack growth direction θ_c, and the crack is extended by two elements (1 mm). Re-meshing is performed automatically and equilibrium is re-established after the crack advances. The process is repeated throughout the crack propagation process until the desired crack propagation length is achieved. Fig. 12(a) shows the initial mesh used in all simulations and Fig. 12(b–d) the meshes generated by FRANC2DL during the crack propagation process for Arcan-specimens with $\Phi = 0^\circ$, 45° and 75°.

The finite element mesh for a DCB specimen with $a/w = 0.423$ is plotted in Fig. 8. This mesh has a total of 2271 six-node triangular plane stress elements.

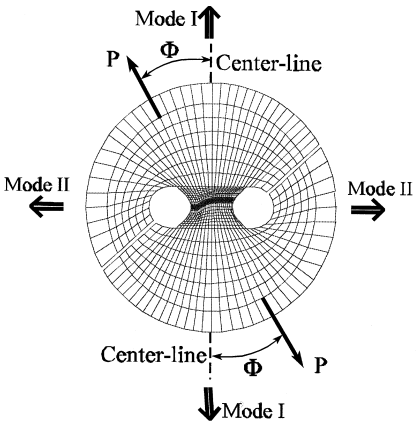

Fig. 10. A typical finite element mesh for an Arcan-specimen, used for a crack growth analysis with a specified crack growth path obtained from an Arcan test.

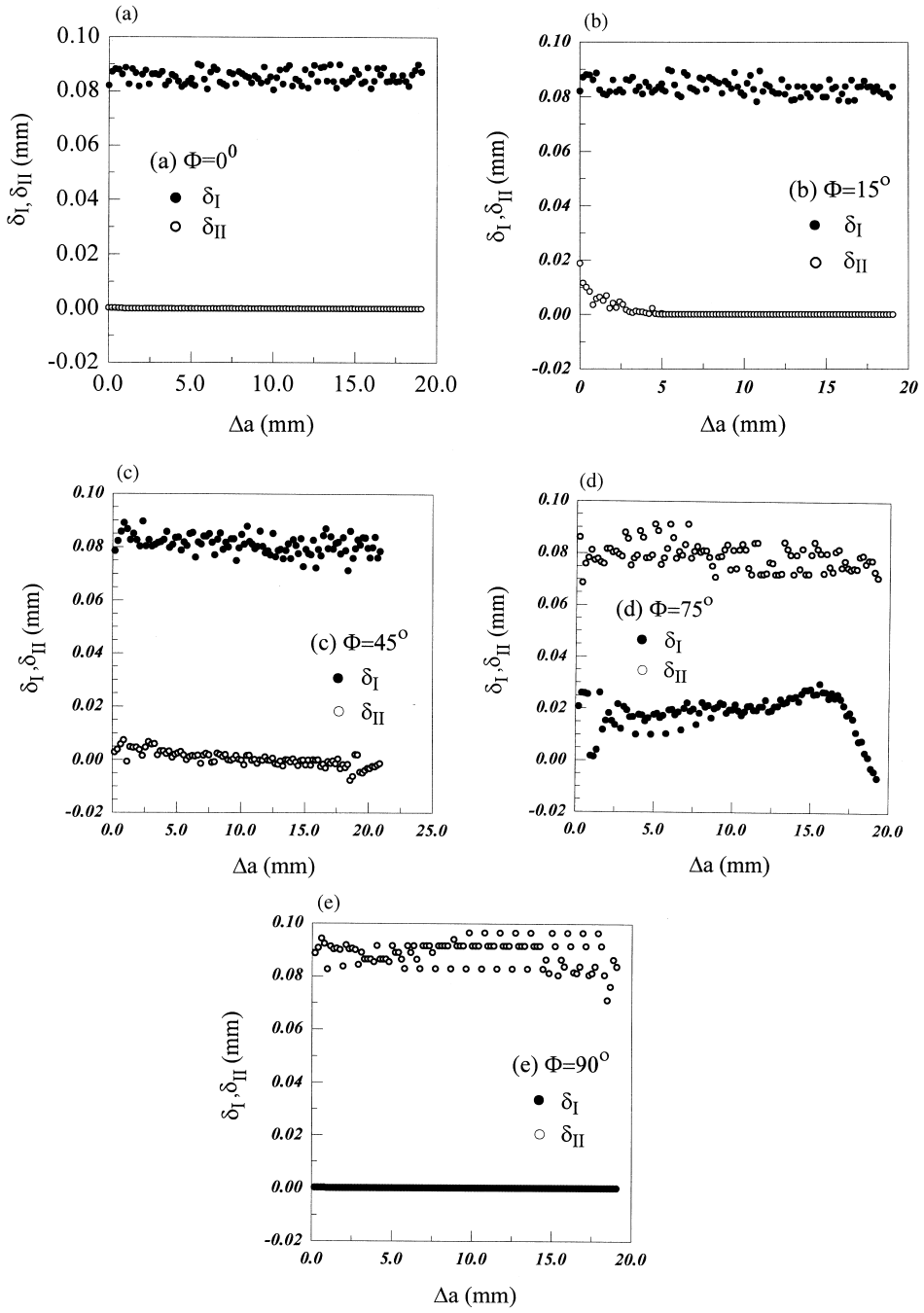

Fig. 11. Computed values of the CTOD components δ_I and δ_{II} during crack growths along experimentally observed crack growth paths for various loading angles: (a) $\Phi = 0°$, (b) $\Phi = 15°$, (c) $\Phi = 45°$, (d) $\Phi = 75°$ and (e) $\Phi = 90°$.

4.2.2. Crack growth simulations for the Arcan specimen without specified paths

Using only the CTOD-based mixed mode fracture criterion, detailed finite element simulations are performed to predict both load-crack extension and load-crack path histories during the entire crack propagation process for $0^\circ \leq \Phi \leq 90^\circ$. During crack propagation, the predicted load-crack extension data and the load-crack path data are computed for all loading angles. Figs. 13 and 14 present comparisons of the experimentally measured and predicted load-crack path and load-crack extension data, respectively, for all loading angles. Results in Fig. 13 demonstrate that crack growth path predictions using a CTOD-based mixed mode fracture criterion are in good agreement with experimental observations throughout the crack propagation process, except at the early stages of crack growth at the transitional loading angle, $\Phi = 75^\circ$. Experimental observations indicate that the crack propagation angle is about 15° during the first 2–3 mm of crack extension, turning to approximately -11° for the remainder of the crack propagation process. The simulation predicts crack propagation along a radial line from initial crack tip at an angle of approximately -13° throughout the crack growth process, which is in excellent agreement with experimental observations for $\Delta a > 3$ mm.

To assess the viability of other crack growth criteria, we cite the recent work by James and Swenson (1998), who used the maximum circumferential stress (MCS) criterion (e.g. see Lee et al., 1997) to predict mode-I dominated ductile crack growth directions under mixed loading conditions. In their simulations, the crack growth direction was predicted using the MCS criterion, and the onset of crack growth was determined using the CTOD criterion, i.e. $D = D_c$. As shown in Fig. 13(a–c) by the dashed

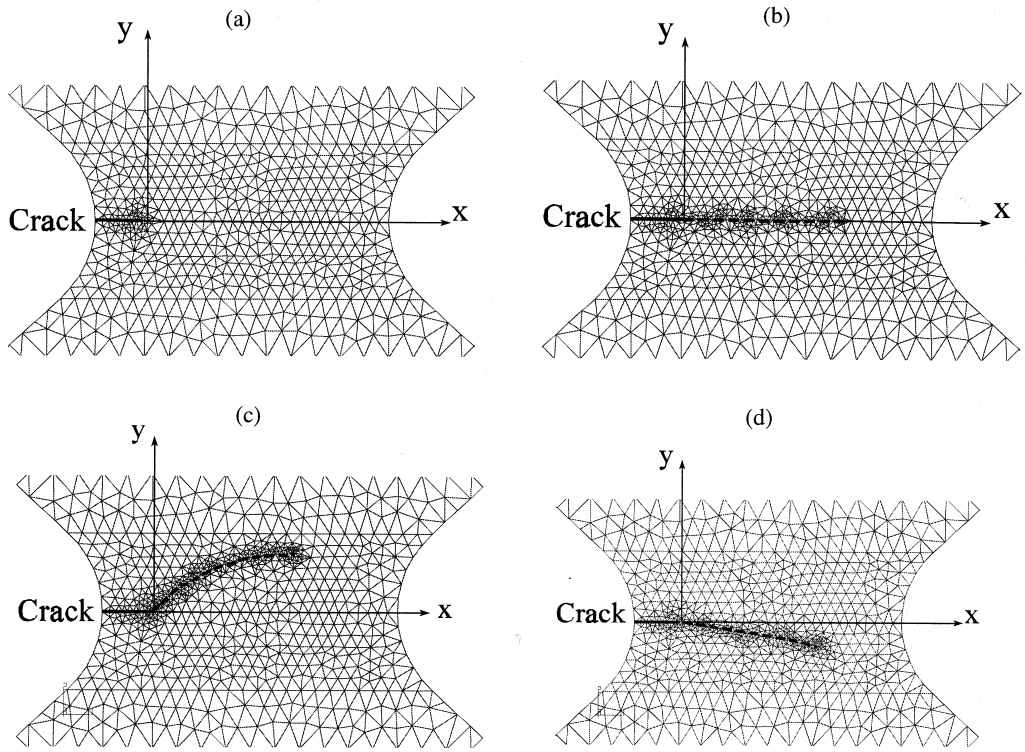

Fig. 12. Near-crack-tip finite element meshes used for crack growth simulations of the Arcan tests without specified crack paths: (a) the initial mesh used in all cases, (b–d) the mesh generated by FRANC2DL during crack growth for $\Phi = 0^\circ$, 45° and 75°, respectively.

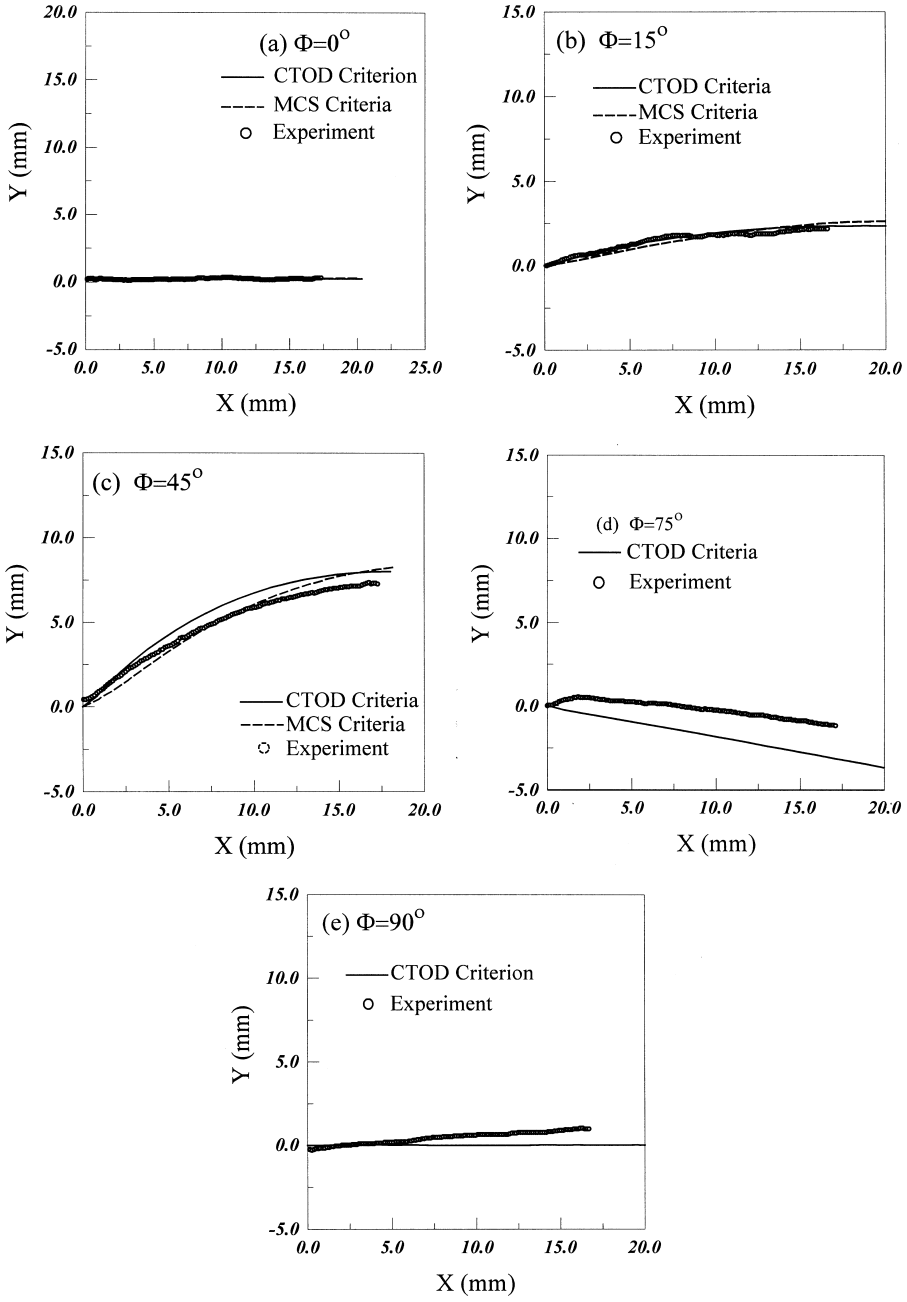

Fig. 13. Predicted and measured crack growth paths for the Arcan tests for (a) $\Phi = 0°$, (b) $\Phi = 15°$, (c) $\Phi = 45°$, (d) $\Phi = 75°$ and (e) $\Phi = 90°$. The MCS criterion predictions in (a–c) are from James and Swenson (1998).

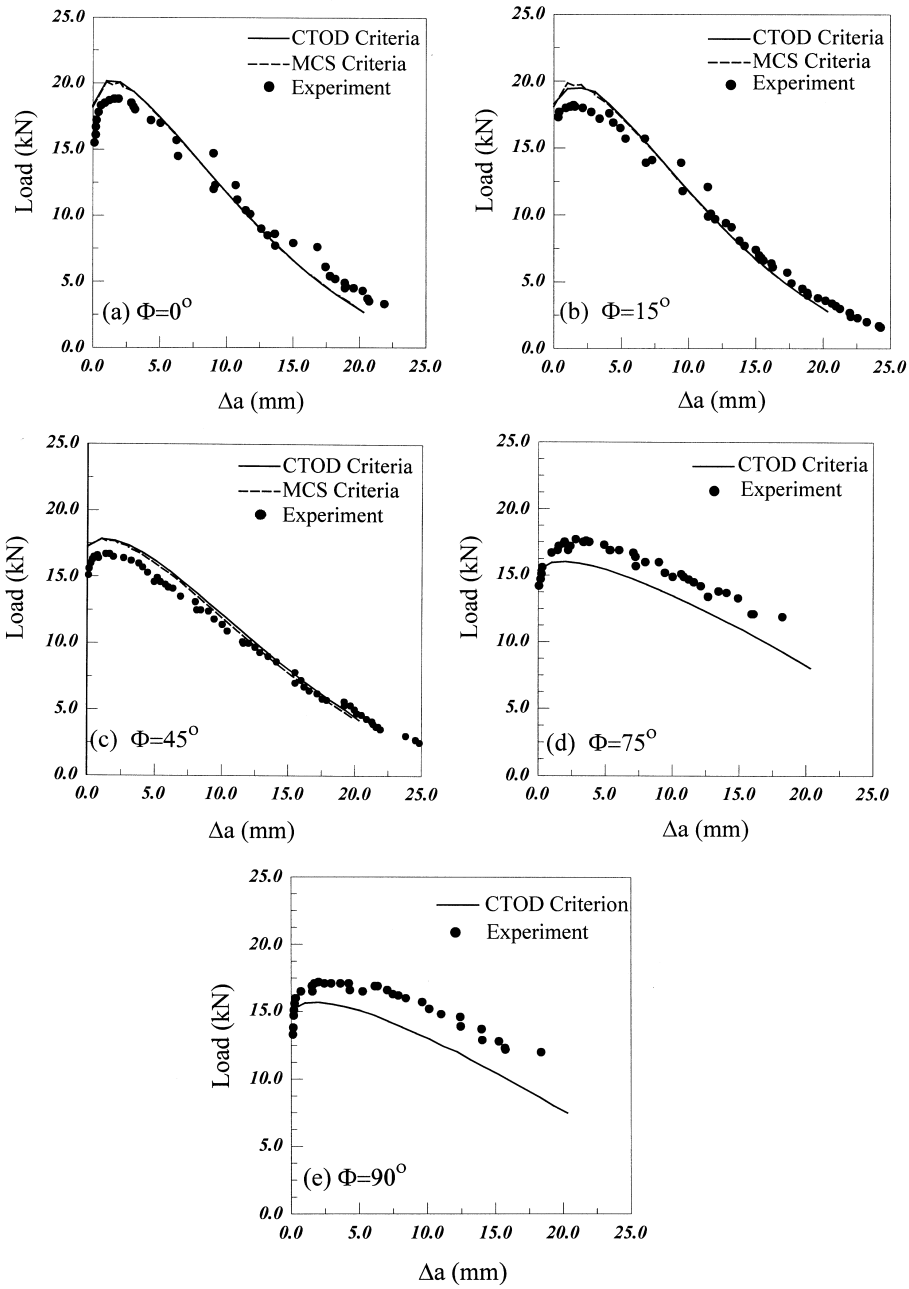

Fig. 14. Predicted and measured load-crack extension curves for the Arcan tests for (a) $\Phi = 0°$, (b) $\Phi = 15°$, (c) $\Phi = 45°$, (d) $\Phi = 75°$ and (e) $\Phi = 90°$. The MCS criterion predictions in (a–c) are from James and Swenson (1998).

line, when crack growth is dominated by Mode I conditions (for $\Phi = 0^\circ$, 15°, 45°), the predicted crack growth path is in good agreement with the actual crack path. However, the MCS direction criterion cannot predict experimentally observed crack growth direction under dominant Mode II conditions (for $\Phi \geq 75^\circ$, 90°) (see Ma et al., 1998). For example, the maximum circumferential stress occurs in the direction of nearly 70° for pure Mode II loading, while the experimentally observed crack growth direction is in its original direction. Furthermore, the MCS criterion requires a much more refined near-tip mesh under elastic-plastic conditions and is much more sensitive to the choice of computational parameters (e.g., the near-tip mesh size and the fixed distance r_c for evaluating the angular variations of the near-tip stress field) than the CTOD criterion.

As shown in Fig. 14, the CTOD-based crack growth criterion leads to overall satisfactory predictions for the load-crack extension curve for the spectrum of mixed mode cases. For $\Phi \geq 75^\circ$, it is observed that the predictions consistently underestimate the test results. One explanation for this under-prediction for $\Phi \geq 75^\circ$ is as follows. For $\Phi \geq 75^\circ$, the crack grows under mode II conditions, with contact occurring all along the fracture surface. Since friction between the crack surfaces increases with crack propagation, an increase in the maximum load is expected. Thus, the numerical simulation should under-predict the maximum load since it does not consider the effect of the friction.

Also shown in Fig. 14(a–c) are the combined MCS-CTOD simulations by James and Swenson (1998) for Mode I dominated crack growth cases ($\Phi = 0^\circ$, 15°, 45°). It is seen that the predictions of the combined MCS-CTOD criterion are nearly identical to the predictions of the mixed-mode CTOD criterion. In fact, this is not surprising because both criteria use CTOD to predict the onset of crack extension, and because, under mode-I dominated conditions, the maximum circumferential stress direction overlays with the direction in which the maximum opening component of CTOD takes place.

4.2.3. DCB crack growth simulations without specified path

Mode I crack growth in DCB specimens is known to have an instability problem, in that the crack growth path is rarely along the expected straight line in the original crack direction. Depending on the particular built-in asymmetry in either the specimen geometry or the loading application, the crack growth path in a DCB test usually will curve away from the straight line either from one side or from the other. Without knowing the details of the built-in asymmetry, it is impossible to predict whether the crack will deviate from the straight line one way or another. Hence, this is a mathematical bifurcation problem.

In this study, the DCB crack growth tests conducted by Pettit (1998) are simulated without the specified crack growth paths. In order for the CTOD criterion to predict the curved crack growth direction, some details of the actual crack-surface geometry of the DCB specimen are modeled in the finite element mesh in Fig. 8, which provides a built-in geometrical asymmetry.

As noted in Section 3, neither the critical CTOD value nor the load-crack extension data were measured during stable tearing of the DCB specimens. However, under the assumption that the CTOD criterion is an appropriate crack growth criterion for this material, the measured load-load point displacement curve and the crack growth path for a particular specimen are used in this study to estimate the critical CTOD value, D_c, for the material. Then the estimated critical CTOD value is used for all later predictions for this and other specimens made of the same material. The procedure used to estimate D_c is as follows.

The results in Section 2 show that for small $|\alpha|(< 10^\circ)$, the $\theta_c \sim \alpha$ relationship predicted by elastic and elastic-plastic analyses are nearly identical. Furthermore, as shown in Eq. (8), the elastic results are independent of material properties. Thus, it is expected that the $\theta_c \sim \alpha$ relation will depend only weakly on material properties for naturally growing cracks when the mode mixity is dominantly mode I ($|\alpha| < 10^\circ$). Using the $\theta_c \sim \alpha$ relation for 2024-T3 aluminum ($a_1 = -36.5$, $b_1 = 2.2$) and assuming a value for D_c, a finite element model similar to the one shown in Fig. 8 is employed with the FRANC2DL code to

simulate the crack growth process for $a/w = 0.171$. By comparing the measured and predicted load-load point displacement curves and the crack growth paths, a critical D_c value with the best overall fit can be chosen.

Using the procedure described above, the DCB specimen with $a/w = 0.171$ is used to derive the critical CTOD value. As shown in Fig. 15 for the load-load point displacement (deflection) curve, and in Fig. 16 for the crack growth path, a best overall fit is found when $D_c \cong 0.1143$ mm. It is noted that experimental measurements A and B in Fig. 16 refer to the crack growth paths measured from the two surfaces of the same DCB specimen. The best overall fit with experimental result is based on the average of the two surface measurements. It is also observed from Fig. 16 that the three predicted crack growth paths curve up on the same side of the original crack line and all can basically follow the measured crack growth trend. The predicted load-crack extension curves for this specimen using the three D_c values are given in Fig. 17. However no test data is available for comparison.

To examine whether the chosen D_c value of 0.1143 mm can be used to produce reasonable predictions for other DCB specimens made of the same material, it is now used in finite element simulations of the crack growth tests in DCB specimens with $a/w = 0.423$ and 0.545. The results are presented in Figs. 18 and 19, where comparisons of the measured and predicted crack growth paths and load-load point displacement curves are shown, respectively. The predicted load-crack extension curves for both specimens are given in Fig. 20. The comparison of the measured and predicted crack paths in Fig. 18 shows that the CTOD criterion does a good job in predicting the rapid changes in the observed crack growth direction, with only slightly less curvature than what was measured. Furthermore, as shown in Fig. 19, the predicted load-load point displacement curve is in excellent agreement with the measured response.

5. Discussion of results

There are several important items to be discussed in more detail in this section, some of which

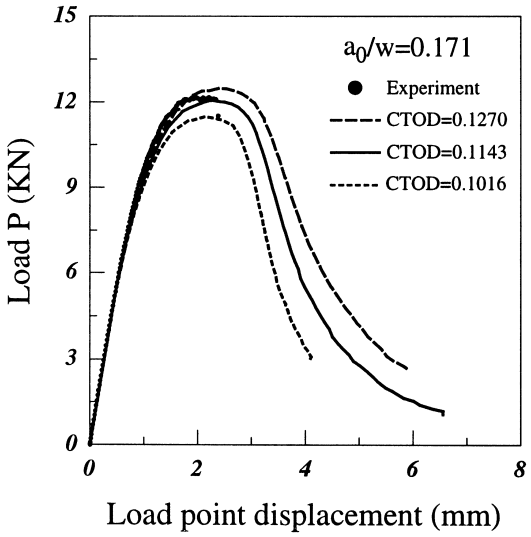

Fig. 15. Predicted and measured load-load-line displacement curves for a DCB specimen with $a/w = 0171$.

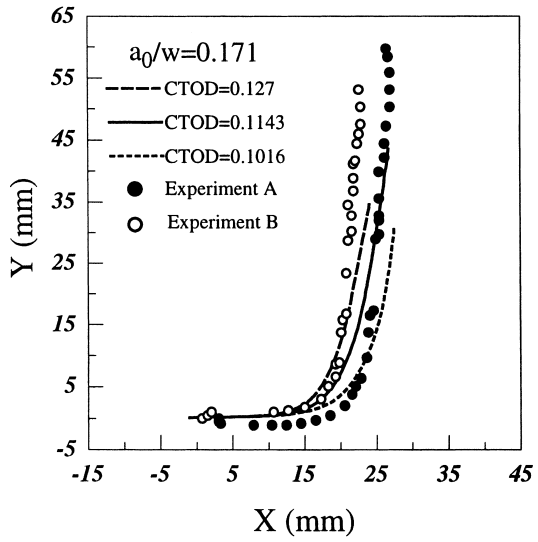

Fig. 16. Predicted and measured crack growth paths for a DCB specimen with $a/w = 0.171$.

are general in context and others specific to the results described above. In the following paragraphs, specific issues are discussed first and general remarks are provided towards the end of the discussion.

5.1. Specific remarks

First, both experimentally measured CTOD data and computer simulations for the Arcan specimen

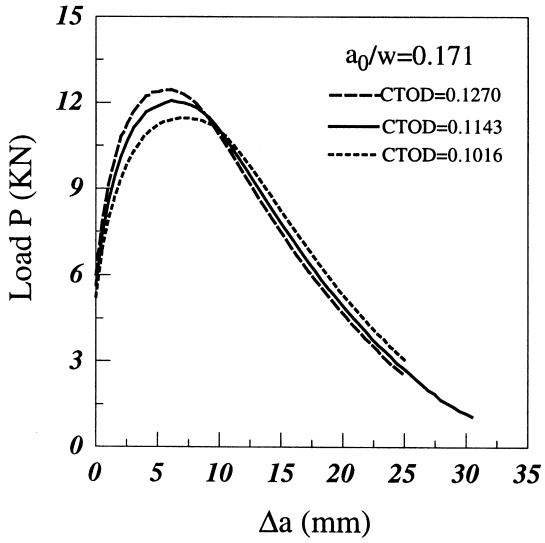

Fig. 17. The predicted load-crack extension curves for a DCB specimen with $a/w = 0.171$.

(using load-crack extension data to extend the crack along pre-specified crack paths) indicate that crack growth occurs under either locally Mode I or locally Mode II conditions. The mode of fracture which occurs depends upon whether the tensile or shear component of CTOD first attains a critical value, as is shown clearly by the change in crack path with loading angle in Fig. 9 and the predicted CTOD values during crack growth shown in Fig. 11(a–d). Based on these results, the CTOD-based mixed mode fracture criterion appears to be appropriate for numerical simulations.

The CTOD-based criterion was used to predict crack growth behavior, including crack growth path,

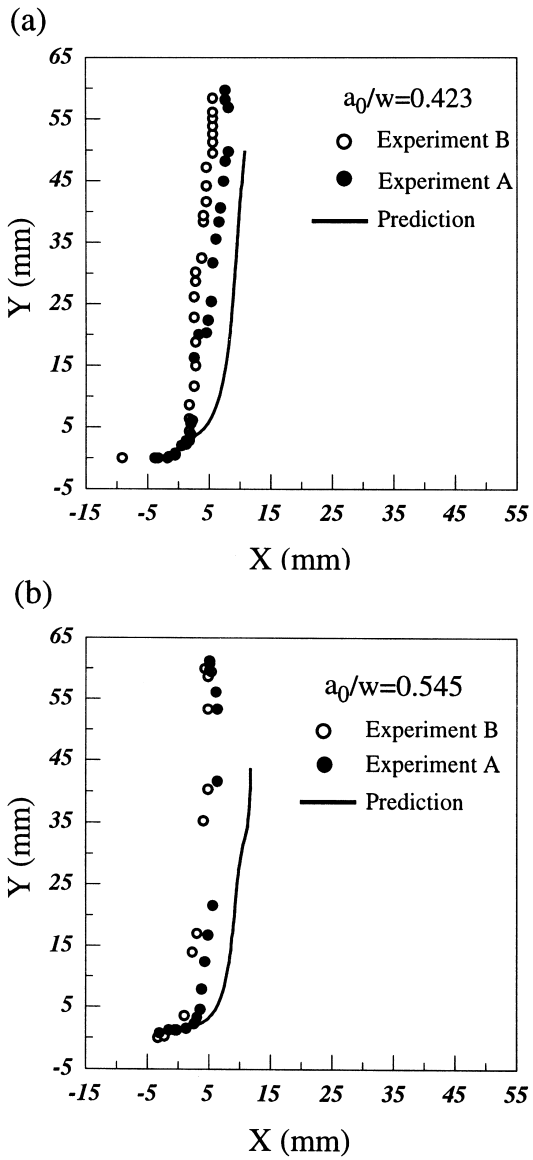

Figs. 18. Predicted and measured crack growth paths for DCB specimens with (a) $a/w = 0.404$ and (b) $a/w = 0.545$, where the predictions are obtained using a critical CTOD of 0.1016 mm.

load-crack growth response and load-load line displacement. Results clearly show that predictions for both the Arcan-specimen and DCB are in good agreement with experimental data. Since the fracture parameter is expected to be a material property, the CTOD criterion developed for 2024-T3 aluminum using the Arcan specimen data can be used for predicting crack growth for other specimen geometry. In fact, we have performed a range of crack growth simulations for both middle crack tension specimens and compact tension specimens machined from 2.3 mm thick, 2024-T3 aluminum. Results similar to

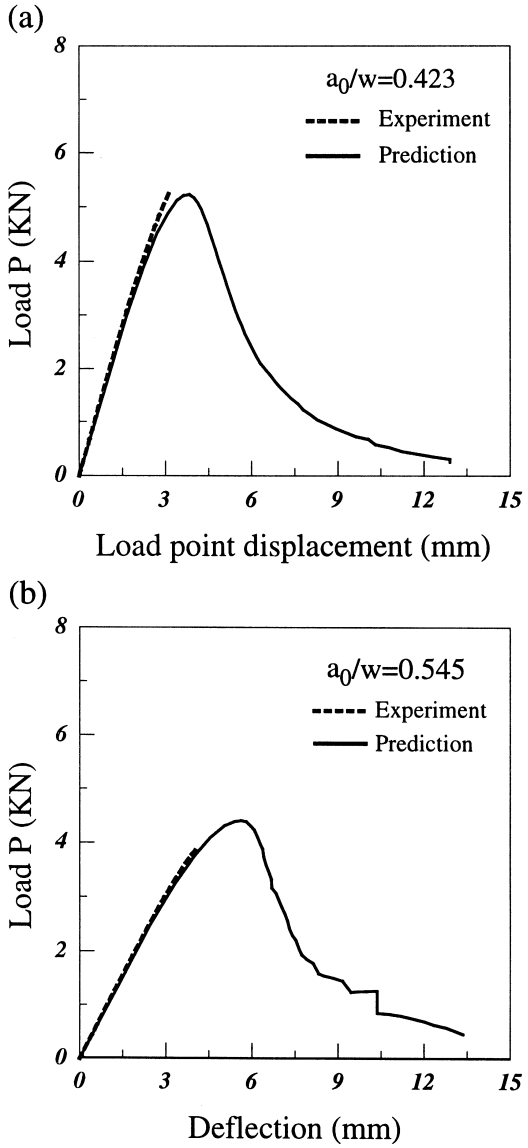

Figs. 19. Predicted and measured load-load-line displacement curves for DCB specimens with (a) $a/w = 0.404$ and (b) $a/w = 0.545$, where the predictions are obtained using a critical CTOD of 0.1016 mm.

those shown in Figs. 12 and 13 for $\Phi \leq 60^\circ$ were obtained for both specimens, with propagation occurring under locally Mode I conditions throughout the crack growth process.

For the DCB specimen reported in Section 4.2.2, due to the lack of a measured critical CTOD, the measured load-load point displacement curve and crack growth path for a particular DCB specimen were used to estimate the critical CTOD value, D_c, under the assumption that the CTOD criterion is an appropriate crack growth criterion for this material. By matching the measured and predicted load-load point displacement curves and also considering the prediction for the crack growth path, an estimate for D_c was determined and used for later predictions for this and other DCB specimens made of the same material. The estimated critical value of CTOD for Al 7050 is approximately on the order of that obtained for Al-2024-T3, with both specimens nominally in the LT orientation (crack initially perpendicular to the rolling direction). Since Al 7050 has a 20% higher yield stress than Al-2024-T3, but nearly elastic-perfectly plastic behavior after yield, the comparison is quite reasonable.

With regard to the crack growth paths shown in Figs. 16 and 18 for the DCB specimen, recent experimental observations of Pettit (1998) suggest that the fracture behavior of Al 7050 is highly anisotropic with $(K_{IC}^{TL}/K_{IC}^{LT}.) \approx 0.60$ for Al-7050, which would imply that $(\delta_{IC}^{TL}/\delta_{IC}^{LT}.) \approx 0.60$. Since our simulations used $\delta_{IC} =$ constant for all angles, it is expected that the predicted crack paths would have less curvature than the actual crack growth paths; this is precisely what is shown in Figs. 16 and 18.

5.2. General remarks

The crack tip opening displacement based mixed mode fracture criterion takes the crack opening displacement at a characteristic distance, r_c, behind the crack tip as fracture parameter. The parameter is somewhat different from previous definitions (e.g. see Shih, 1981; Tracey, 1976) of crack tip opening displacement, δ_t. These definitions demonstrate that δ_t is equivalent to the J-integral for stationary flaws. The characteristic distance used in this work is about 1 mm, which is based on experimental data obtained for 2024-T3 aluminum. The distance appears to be an important factor in using the CTOD

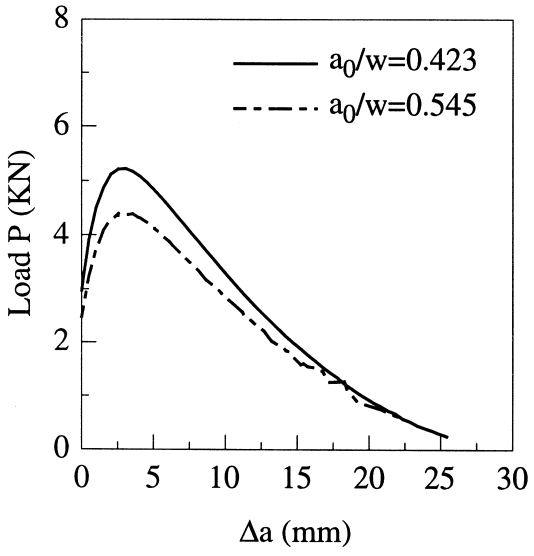

Fig. 20. The predicted load-crack extension curves for DCB specimens with $a/w = 0.404$ and $a/w = 0.545$.

criterion for predicting the onset and direction of crack growth. If the distance is too small, the crack opening displacement does not scale the deformations in the crack tip region, which determines the onset and continuation of crack growth. On the other hand, if the distance is too large, the crack opening displacement will include contributions of deformations in the remote field. Thus, the crack opening displacement must be measured at a characteristic distance for describing onset and direction of crack growth, which is most likely material dependent.

The CTOD-based fracture criterion can be extended to include the effects of anisotropic material fracture behavior (e.g. Al 7050) simply by including a functional form for the critical CTOD that varies with direction. The functional form can be determined experimentally through a series of mixed mode tests. The specimens to be tested would have flaws at an initial angle to the material directions, and the effects of material direction on critical CTOD would be measured during crack growth using full-field methods such as digital image correlation used by Amstutz *et al*. to quantify both components of critical CTOD during crack growth.

Much of the experimental work involving CTOD and mixed mode fracture has focused on thin sheet material. For example, Dawicke and Sutton (1994) and Amstutz et al. (1995a, 1995b) have shown that the crack front attains a stable shape and CTOD is essentially constant for crack growth greater than the specimen thickness. Thus, plane stress crack growth simulations were used successfully in all of the analyses presented in this work. With regard to the use of a CTOD criterion for predicting stable crack growth in thick structural components, if the critical CTOD is truly a material parameter, then the effects of specimen geometry would primarily affect the 'driving force' and the CTOD's extension for use in three-dimensional simulations is plausible. In this regard, recent work by Lloyd and Piascik (1995) has shown that the critical CTOD during locally Mode I crack growth is nearly constant through the thickness of the specimen for crack growth greater than the specimen thickness. During the very earliest stages of crack growth, CTOD remained constant throughout the interior of the specimen, with an apparent rise in CTOD occurring very near the specimen surface. Though suggestive, it is clear that additional experimental and computational work will be required to determine the generality of the criterion.

For those through-thickness flaws where plane stress does not adequately describe crack tip constraint during stable crack growth, it is possible to approximate the mixed state-of-stress in the crack tip region through use of a 'plane strain core' (see Newman, 1977, 1984) or full three-dimensional analyses (see Newman et al., 1992). To implement the 'plane strain core' in a two-dimensional analysis, plane strain is assumed in a region immediately surrounding the crack tip whereas plane stress is held outside this near-tip region. Since high stress triaxiality occurs in the crack tip region, at least around the mid-section of a planar crack front for locally Mode I conditions, enhanced void growth and coalescence in the crack tip region would be expected to occur. Thus, the load-carrying capacity of material in crack tip region will decrease with increasing loading since attainment of a critical CTOD value would be easier in the increasingly-damaged material. Thus, incorporating crack tip constraint (e.g. plane strain core, 3D models) and damage concepts into the FEM analyses should provide the basis for extending the range of applications for the CTOD-based criterion. For example, predictions based on these models would most likely improve the predictions of (a) maximum load in Figs. 14 and 19 by reducing the load-carrying capability as damage occurs in the crack-tip region and (b) initial crack path in Fig. 13 at the transition angle, where the effects of constraint are most likely important.

Acknowledgements

The authors wish to thank (a) Mr. Rick Pettit from Boeing, Inc. for both the use of his experimental data from several DCB crack growth tests and his timely discussions of key issues in the testing process,

(b) Dr. Daniel Swenson from Kansas State University for his assistance in modifying and using FRANC2DL in our fracture simulations and (c) Dr. David S. Dawicke at NASA Langley Research Center for his assistance in both fracture tests and fracture simulations. In addition, the financial support of NASA headquarters through the South Carolina EPSCoR grant NCC5-174 is gratefully acknowledged.

References

Amstutz, B.E., Sutton, M.A., Dawicke, D.S., Newman Jr., J.C., 1995a. An experimental study of CTOD for mode I/II stable crack growth in thin 2024-T3 aluminum specimens. Fracture Mechanics ASTM STP 1256, 256–271.

Amstutz, B.E., Sutton, M.A., Dawicke, D.S., Boone, M.L., 1995b. Effects of mixed mode I/II loading and grain orientation on crack initiation and stable tearing in 2024-T3 aluminum. Fatigue and Fracture ASTM STP 1296, 105–125.

Arcan, M., Hashin, Z., Voloshin, A., 1978. A methods to produce uniform plane stress state with applications to fiber-reinforced materials. Experimental Mechanics 18, 141–146.

Begley, J.A., Landes, J.D., 1972. The J-integral as a fracture criterion. Fracture Toughness, Part II ASTM STP 560, 170–186.

Bruck, H.A., McNeill, S.R., Sutton, M.A., Peters, W.H., 1989. Determination of surface deformations using digital image correlation with the Nnewton Raphson method for partial differential corrections. Experimental Mechanics 29, 261–267.

Chao, Y.J., Sutton, M.A., 1994. On the fracture of solids characterized by one or two parameters: theory and practice. Journal of the Mechanics and Physics of Solids 42, 629–647.

Clarke, G.A., Andrews, W.R., Schmidts, D.W., Paris, P.C., 1976. Single specimen tests for J_{IC} determination. Mechanics of Crack Growth ASTM STP 590, 27–42.

Cotterell, B., Rice, J.R., 1980. Slightly curved or kinked cracks. International Journal of Fracture 16, 155–169.

Dawicke, D.S., Sutton, M.A., 1994. CTOA and crack-tunneling measurements in thin 2024-T3 aluminum alloy. Experimental Mechanics 34, 357–368.

Dawicke, D.S., Sutton, M.A., Newman Jr., J.C., Bigelow, C.A., 1995. Measurement and analysis of critical CTOA for aluminum alloy sheet. Fracture Mechanics ASTM STP 1220, 358–379.

Deng, X., Newman, J.C.Jr., 1997a. Implementation and application of a large-rotation finite element formulation in NASA code ZIP2DL. In: FAA-NASA Symposium on Continued Airworthiness of Aircraft Structures, Atlanta, Georgia, August 28–30 1996, vol. II, pp. 377–390 DOT/FAA/AR-97/2.

Deng, X., Newman, J.C.Jr., 1997b. ZIP2DL — An Elastic-Plastic, Large-Rotation Finite-Element Stress Analysis and Crack-Growth Simulation Program. NASA Langley Research Center (NASA Technical Memorandum 110332).

Erdogan, F., Sih, G.C., 1963. On the crack extension in plates under plane loading and transverse shear, Transactions of the ASME. Journal of Basic Engineering 85, 519–527.

Hallback, N., Nilsson, F., 1994. Mixed mode I/II fracture behavior of an aluminum alloy. Journal of the Mechanics and Physics of Solids 42, 1345–1374.

Han, G., Sutton, M.A., Chao, Y.J., 1994. A study of stationary crack tip deformation fields in thin sheets by computer vision. Experimental Mechanics 34, 125–141.

Han, G., Sutton, M.A., Chao, Y.J., 1995. A study of stable crack growth in thin SEC specimens of 304 stainless steel. Engineering Fracture Mechanics 52, 525–555.

Hancock, J.W., Reuter, W.G., Parks, D.M., 1993. Constraint and toughness parameterized by T. Constraint Effects in Fracture ASTM STP 1171, 41–63.

Hutchinson, J.W., Paris, P.C., 1979. Stability analysis of J-controlled crack growth. Elastic-plastic fracture ASTM STP 668, 37–64.

James, M.A., Swenson, D. 1998. A software framework for two-dimensional mixed mode I/II elastic-plastic fracture. In: Miller (Ed.), Mixed Mode Crack Behavior ASTM STP 1359, (in press).

Kanninen, M.F., Rybicki, E.F., Stonesifer, R.B., Broek, D., Rosenfiels, A.R., Marschall, C.W., Hahn, G.T., 1979. Elastic-Plastic fracture mechanics for two-dimensional stable crack growth and instability problems. Elastic-plastic fracture ASTM STP 668, 121–150.

Larsson, S.G., Carlsson, A.J., 1973. Influence of non-singular stress terms and specimen geometry on small-scale yielding at crack tip in elastic-plastic materials. Journal of the Mechanics and Physics of Solids 21, 263–278.

Lee, K., Lee, J.D., Liebowitz, H., 1997. Finite element analysis of the slow crack growth process in mixed mode fracture. Engineering Fracture Mechanics 4, 551–577.

Lloyd, W.R., Piascik, R.S., 1995. Three-dimensional crack growth assessment by microtopographic examination. Fracture Mechanics: ASTM STP 1256 26, 303–318.

Ma, F., Deng, X., Sutton, M.A., Newman Jr, J.C. 1999. A CTOD based mixed mode fracture criterion. In: Mixed Mode Crack Behavior, pp. 86–110.

Maccagno, T.M., Knott, J.F., 1991. The low temperature brittle fracture behavior of steel in mixed modes I and II. Engineering Fracture Mechanics 38, 111–128.

Maccagno, T.M., Knott, J.F., 1992. The mixed mode I/II fracture behavior of lightly tempered HY130 steel at room temperature. Engineering Fracture Mechanics 41, 805–820.

Newman Jr., J.C., 1977. Finite element analysis of crack growth under monotonic and cyclic loading. ASTM STP 637, 56–80.

Newman Jr., J.C., 1984. An elastic-plastic finite element analysis of crack initiation, stable crack growth, and instability. Fracture Mechanics STP 833, 93–117.

Newman, J.C.Jr., Dawicke, D.S., Bigelow, C.A., 1992. Finite Element Analyses and Fracture Simulation in Thin Sheet Aluminum Alloy NASA TM-107662.

Nuismer, R.J., 1975. An energy release rate criterion for mixed mode fracture. International Journal of Fracture 11, 245–250.

Palaniswamy, K., Knauss, W.G., 1978. On the problem of crack extension in brittle solids under general loading. In: Nemat-Nasser, S. (Ed.), Mechanics Today, vol. 4. Pergamon Press, pp. 87–148.

Paris, P.C., Taha, H., Zahoor, A., Ernst .19, H., 1979. The theory of instability of the tearing mode of elastic-plastic crack growth. Elastic-plastic fracture ASTM STP 668, 5–36.

Pawliska, P., Richard, R.H., Kiekmann, P., 1993. The behavior of cracks in elastic-plastic materials under plane normal and shear loadings. International Journal of Fracture 62, 43–54.

Pettit, R., 1998. Private Communication with M.A. Sutton.

Rice, J.R., 1974. Limitations to the small scale yielding approximation for crack tip plasticity. Journal of the Mechanics and Physics of Solids 22, 17–26.

Rice, J.R., Sorensen, E.P., 1978. Continuing crack tip deformation and fracture for plane strain crack growth in elastic-plastic solids. Journal of the Mechanics and Physics of Solids 26, 163–186.

Roose, E., Eisele, U., Silcher, H., 1993. Effect of stress state on the ductile fracture behavior of large-scale specimens. Constraint Effects in Fracture ASTM STP 1171, 41–63.

Shih, C.F., deLorenzi, H.G., Andrews, W.R., 1979. Studies on crack initiation and stable crack growth. Elastic-Plastic Fracture ASTM STP 668, 65–120.

Shih, C.F., 1981. Relationship between the J-integral and the crack opening displacement for stationary and extending cracks. Journal of the Mechanics and Physics of Solids 29, 305–326.

Sih, G.C., 1974. Strain energy-density factor applied to mixed mode crack problem. International Journal of Fracture 10, 305–321.

Sih, G.C., Liebowitz, H., 1968. Mathematical theories of brittle fracture. In: Liebowtz, H. (Ed.), Fracture, An Advanced Treatise, vol. 2. Academic Press, pp. 67–190.

Sumi, Y., Nemat-Nasser, Y., Keer, L.M., 1985. On crack path stability in a finite body. Engineering Fracture Mechanics 22, 759–771.

Sutton, M.A., McNeill, S.R., Jang, J., Babai, M., 1988. The effects of subpixel image restoration on digital correlation error estimates. Optical Engineering 27, 173–185.

Sutton, M.A., Zhao, W., Boone, M.L., Reynolds, A.P., Dawicke, D.S., 1997a. Prediction of crack growth for mode I/II loading using small-scale yielding and void initiation/growth concepts. International Journal of Fracture 83, 275–290.

Sutton, M.A., Zhao, W., Deng, X., Dawicke, D.S., Newman, J.C.Jr., 1997b. Numerical Investigations Into the Viability of CTOD as a Fracture Parameter for Mixed-Mode I/II Tearing of Thin Aluminum Sheets. In: Proceedings of the FAA-NASA Symposium on Continued Airworthiness of Aircraft Structures, Atlanta, Georgia, August 28–30 1996, vol. II, pp. 461–472 DOT/FAA/AR-97/2.

Swenson, D., James, M., 1997. FRANC2D/L: A Crack Propagation Simulator for Plane Layered Structures, User's Guide, Version 1.4.

Tracey, D.M., 1976. Finite element solutions for crack tip behavior in small scale yielding. ASME Journal of Engineering Materials and Technology 98, 146–151.

Well, A.A., 1961. Unstable crack propagation in metals: cleavage and fast fracture. Proceedings of the Cranfield Crack Propagation Symposium 1, 210–230.

Yang, S., Chao, Y.J., Sutton, M.A., 1993. Higher order asymptotic crack tip fields in a power law hardening material. Engineering Fracture Mechanics 45, 1–20.